THE JOURNAL OF PHYSICAL CHEMISTRY A
A JOURNAL OF THE AMERICAN CHEMICAL SOCIETY

pubs.acs.org/JPCA Article

# The Elusive Bound OH-Stretching First Overtone of Water Dimer

*Published as part of The Journal of Physical Chemistry A special issue "John F. Stanton Memorial Issue".*

Henrik G. Kjaergaard,* Emil Vogt, Alexandr S. Bogomolov, and Clément Lauzin*

Cite This: https://doi.org/10.1021/acs.jpca.5c07868 Read Online

ACCESS | Metrics & More | Article Recommendations | Supporting Information

**ABSTRACT:** Water dimer is a classical example of an OH···O hydrogen bound complex and plays a critical role in the atmosphere. The bound OH-stretching ($OH_b$) fundamental transition displays the characteristic wavenumber redshift and intensity enhancement, observed repeatedly under many different experimental conditions. In contrast, the first $OH_b$-stretching overtone is predicted to be several orders of magnitude weaker in intensity. Recent full-dimensional ro-vibrational calculations have revised earlier theoretical predictions, suggesting that the $OH_b$-stretching first overtone may exhibit an intensity comparable to that of other observed OH-stretching transitions at these higher wavenumbers. Using jet expansion cavity ring-down spectroscopy in the predicted spectral region, we successfully observed this previously elusive transition. The observed transition wavenumber, intensity, and band shape show excellent agreement with the new theoretical predictions. The overlap of many closely lying ro-vibrational transitions, even at the cold temperature of the jet, gives rise to a relatively unstructured broad band. We determine the experimental $OH_b$-stretching first overtone vibrational band origin to be 7049 $cm^{-1}$ and estimate the lifetime to be about 10 ps.

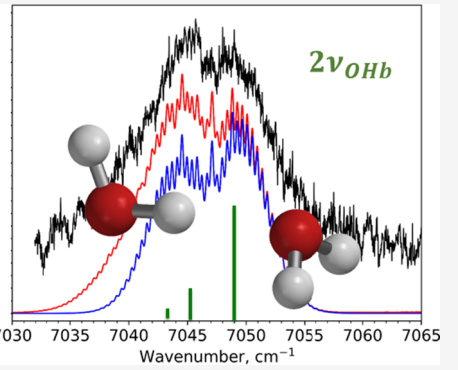




## INTRODUCTION

Water derives its unique properties from the hydrogen bonds that hold the water molecules together. To have any hope of understanding liquid water, we need to be able to fully understand the smallest water cluster, the water dimer, $H_2O{\cdot}H_2O$ (Figure 1). The water dimer is in itself also important in,

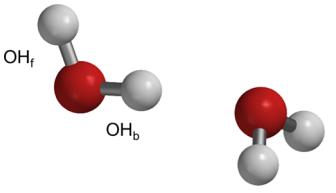


**Figure 1.** Structure of the water dimer. The two hydrogen atoms in the water acceptor unit are equivalent, while the free, $OH_f$, and bound, $OH_b$ of the donor unit are different. The principle *a*-axis lies close to the O−O axis and the $OH_b$ bond is close to parallel with the *a*-axis.

for example, the radiative transfer of the Earth's atmosphere.[1,2] The so-called water self-continuum is an empirical function that model the radiative transfer of water and which scales with the water pressure squared, as expected for the water dimer abundance. However, the physical understanding of this continuum is still under debate.[2,3] In addition, nucleation and growth of particles in the atmosphere depend on interaction with and aggregation of water molecules. The strength of the interaction between the two water units in the water dimer is an essential parameter in this process.

Spectroscopy and theory have gone hand in hand to enhance our understanding of the water dimer, with the ro-vibrational spectra of water dimer proving more challenging than one intuitively would expect for such a small system. Since the first infrared observation of water dimer in an $N_2$ matrix in 1957,[4] numerous more and more advanced ro-vibrational spectra and theoretical models of water dimer have appeared.[3] The bound OH-stretch, $OH_b$, is perhaps the most interesting vibration as its properties relate to the hydrogen bond. The $OH_b$-stretching fundamental transition exhibits a wavenumber redshift and intensity enhancement, characteristic features associated with a hydrogen bond.[5−7] These features facilitate its detection, and in cold gas-phase jet-expansion spectra it is observed at 3601 $cm^{-1}$.[8,9] The first infrared cavity ring down detection of the $OH_b$-stretching transition appeared in 1997.[10] The hydrogen bond is strongly affected by the matrix environment and the $OH_b$-stretching transition is usually observed at lower wavenumbers in matrix isolation experiments. For example, in $N_2$ matrix experiments it is observed at 3550 $cm^{-1}$ (Table

Received: November 18, 2025
Revised: January 6, 2026
Accepted: January 7, 2026

S1).[11] In jet experiments, formation of clusters is favored and higher order clusters often appear. Their signals have occasionally been assigned to water dimer confusing and reigniting a debate associated with the assignment of the fundamental $OH_b$-stretching transition. However, it seems that this conundrum is now unequivocally solved with the transition at 3601 $cm^{-1}$ in the jet expansion assigned to the fundamental $OH_b$-stretching transition, $\nu_{OH_b}$.[12−14]

Theoretical models of water dimer are complicated due to the importance of coupling between the high-frequency intramolecular modes and the low-frequency large amplitude motions. The low-frequency modes perturb the hydrogen bond and enable the interchange of the hydrogen atoms, leading to tunneling splitting. Comparison of reduced dimensionality OH-stretching and full dimensionality VPT2 (vibrational perturbation theory to second order) calculations indicated clearly the importance of these low-frequency modes on the OH-stretching transition in particular the $OH_b$-stretching transitions.[15] Over the years, the vibrational models have increased in dimension and complexity; from simple 2D + 2D, 3D + 3D (including only intramolecular modes), to 6D +6D (adiabatically separating the 6 high and 6 low energy vibrations), to full dimensional models.[16−22] Whereas full dimensional models couple all vibrations, their accuracy is typically limited by the level of basis set convergence. Recently, such models have been used to compute excited OH-stretching states of water dimer.[3,20,23] The calculated wavenumbers and relative intensities of the four fundamental OH-stretching transitions ($\nu_{OH_b}$, $\nu_{OH_+}$, $\nu_{OH_f}$, $\nu_{OH_-}$) have been found to be in good agreement with observations, thus enabling an unequivocal assignment.[3]

In the first OH-stretching overtone region, the number of states increases dramatically and observation of the first $OH_b$-stretching overtone has been much more elusive. In the near-infrared $N_2$ and Ar matrix experiments, the first $OH_b$-stretching overtone transition was not detected.[24,25] Already in the early reduced dimensional (2D and 3D) vibrational calculations, the first $OH_b$-stretching overtone transition was indeed found to be very weak.[16,17] This was attributed to a cancellation of the contribution to the intensity from the first (linear) and second (quadratic) term in the expansion of the dipole moment function in the curvilinear internal OH-stretching coordinate.[26] Due to this cancellation, the intensity of this overtone was not surprisingly found to be sensitive to the choice of vibrational model and electronic structure method (Table S2).[3,15,27,28] In a subsequent Ne matrix experiment, the fundamental $OH_b$-stretching transition was observed at 3590 $cm^{-1}$, and a weak transition at 7018 $cm^{-1}$ (both as split doublets) with an observed intensity of about $2 \times 10^{-3}$ that of the fundamental $OH_b$-stretching transition was assigned to the first $OH_b$-stretching overtone.[11] In the Ne matrix, the fundamental $OH_b$-stretching transition is around 11 $cm^{-1}$ lower than the observed gas-phase jet expansion value, whereas the other three fundamental OH-stretching transitions are found at higher wavenumbers compared to the jet expansion observations. Despite this early assignment in the Ne matrix experiments, no gas-phase jet expansion detection has followed.

Rotationally resolved spectra in the first OH-stretching overtone region have been observed in jet expansion experiments in the 7100−7300 $cm^{-1}$ region at about 7 ± 3 K, and in the 7188−7285 and 7357−7386 $cm^{-1}$ regions at about 10 ± 3 K.[29,30] By combining a 12D vibrational model based on *n*-mode approximations of operators in internal coordinates with a rotation-tunneling model, transition wavenumbers and intensities were recently computed in the first OH-stretching overtone region.[21] Observed bands were conclusively assigned and vibrational band origins were determined for three of the four OH-stretching transitions ($2\nu_{OH_b}$, $2\nu_{OH_+}$, $2\nu_{OH_f}$, $2\nu_{OH_-}$). The $OH_b$-stretching overtone transition is predicted, both from calculations and the Ne matrix experiments, to be outside the range covered by the lasers of the previous experiments. In these earlier jet expansion experiments, one OH-stretching combination transition was observed at 7366 $cm^{-1}$.[29] It is assigned to the $\nu_{OH_b} + \nu_{OH_f}$ transition and corresponds to the predicted most intense of the six OH-stretching combination transitions.[21] From the computation, the intensity of the first $OH_b$-stretching overtone band, $2\nu_{OH_b}$, is predicted to be similar to that of the observed OH-stretching combination band and the observed $2\nu_{OH_+}$ band.[21]

Here, we present cavity ring-down spectra of the water dimer in the wavenumber region near the predicted $OH_b$-stretching first overtone transition. A narrow band diode laser was procured to record cavity ring-down spectra centered around to the predicted wavenumber region. A distinct band is observed whose intensity, profile, and position closely match theoretical predictions, enabling an unambiguous assignment to the $OH_b$-stretching first overtone. Comparison between simulated and experimental spectra yields an estimated rotational temperature of approximately 20 K, a vibrational band origin at 7049 $cm^{-1}$, and a lifetime of about 10 ps. Accurate experimental transition wavenumbers are essential for testing and refining potential energy and dipole moment surfaces, with vibration−rotation tunneling (VRT) transitions serving as a sensitive probe for the weak intermolecular interactions between the two water units.[18−20,22] For the water dimer, the spectra reported here and in refs 29 and 30 in the OH-stretching first overtone region are particularly valuable for understanding couplings between intra- and intermolecular vibrations. From the perspective of the intramolecular modes, coupling to the low-frequency intermolecular motions leads to perturbations in both transition wavenumbers and intensities. Conversely, from the viewpoint of the intermolecular modes, the coupling to intramolecular vibrations gives rise to VRT energy level patterns that depend on the specific OH-stretching excitation. As a consequence, reliable determination of quantities such as vibrational band origins demands accurate spectral simulations to guide the analysis of the observed congested spectra.

Other mentionable observations of bound XH-stretching first overtones in hydrogen bound complexes include the HF dimer and the OH···O bound methanol, ethanol and *tert*-butyl alcohol dimers. For the HF dimer, the $\Delta K_a = 0$ transition of the bound FH-stretch was observed at 7550.3555(26) $cm^{-1}$ using continuous-wave-diode laser cavity ring-down spectroscopy in a pulsed supersonic slit jet expansion. The lifetime was estimated to be about 50 ps, compared with the much longer lifetime of about 1.6 ns for the acceptor FH-stretching first overtone, highlighting the nonstatistical and mode-selective predissocation behavior even at these energies far above the dissociation threshold.[31] For the alcohol dimers, the bound OH-stretching transitions were observed with Fourier transform infrared spectroscopy also in supersonic expansions. The


https://doi.org/10.1021/acs.jpca.5c07868
J. Phys. Chem. A XXXX, XXX, XXX−XXX

observed intensities relative to the corresponding $OH_b$-stretching fundamental transitions were 0.004−0.001, highlighting the weak intensity of the first overtone, compared with the fundamental transition of this local oscillator.[32]

## METHODS

### Experimental Details

The measurements were performed using the FANTASIO experimental setup,[33,34] now located in Louvain-la-Neuve, Belgium. Water dimer was produced in a supersonic gas expansion using an 80 mm × 50 $\mu$m pulsed slit valve.[35] The controlled evaporator mixer (Bronkhorst F-201CV-2K0-RAD-11-V gas flow controller and M13-RAD-11−0 liquid flow controller) was used to adjust the water to Argon relative densities. The flows were 3 standard L/min for argon and 1.7 mL/h for liquid distilled water ($H_2O$). The gas was pulsed at 4 Hz with a pulse duration of 20 ms and a backing pressure of 1 bar. The water dimer spectrum was recorded using the cavity ring-down spectrometer (CRDS) of the FANTASIO setup.[35] The laser source of the spectrometer was a DFB laser of a few MHz line width (PL-DFB-1418-A-A81-SA from Nano-Giga/LD-PD INC, 25 mW output). The laser was tuned over around 30−40 $cm^{-1}$ by varying the temperature of a Peltier cell. About 10% of the laser power was used to record an etalon signal for frequency calibration. The rest was amplified by a booster optical amplifier (BOA1410S from Thorlabs) to reach a power of 250 mW. The CRDS cavity formed by two highly reflective mirrors (140989 from Layertec) was aligned with the first-order output (120 mW) of an acousto-optical modulator. The empty cavity ring-down (RD) time was ∼105 $\mu$s. The RDs were sorted into data sets corresponding to measurements with and without gas expansion. Those were measured from 5 to 20 ms and from 70 to 248 ms, respectively, after the valve opening signal.[36] At least 20 RDs were averaged for each spectral point. The spectrum was frequency calibrated using a stable etalon[35] interferometric signal and water monomer lines[37] present in the studied spectral range.

Spectra in the 7030−7065 $cm^{-1}$ range were measured slow with a large number of RDs per point and fast with a minimal number of RDs. In both cases, the spectrum did not present any visible rotational structure. The $H_2O$ monomer lines presented in the range are removed from the experimental spectrum. Only the fast spectra are presented. Indeed, those were measured in a reduced amount of time allowing us to minimize the influence of long-term drift of the experimental conditions and any resulting asymmetry of the recorded band. Examples of different scans are shown before and after baseline correction in Figure S1.

We also compared the spectrum in the 7030−7065 $cm^{-1}$ range with a spectrum in the region from 7175−7240 $cm^{-1}$ recorded under similar conditions,[35] to facilitate comparison of the relative intensities of the transitions in the two segments of the OH-stretching first overtone region (Figure S2).

### Theory and Simulation

The first overtone $OH_b$-stretching spectrum was simulated using computed results from ref 21. To account for the increased experimental temperature (∼20 vs ∼10 K), Boltzmann weights (of rotation-tunneling states) were adjusted, and new rotational profiles were simulated (Tables S3−S5). In ref 21, vibrational band origins and intensities were calculated with a 12D vibrational model in internal coordinates, denoted VibMeMIC. The vibrational transition intensities from state $i$ to $j$ is expressed as the unitless oscillator strength by[26]

$$f_{j\leftarrow i} = 4.702 \times 10^{-7}\ [\mathrm{cmD}^{-2}]\ \tilde{\nu}_{j\leftarrow i} |\langle \Psi_j | \vec{\mu} | \Psi_i \rangle|^2 \quad (1)$$

where $\tilde{\nu}$ is the transition wavenumber in $cm^{-1}$, $\Psi_i$ and $\Psi_j$ are the initial and final state wave functions and $\vec{\mu}$ is the dipole moment function in Debye (1D = 3.33564 × $10^{-30}$ cm). In VibMeMIC, the potential energy, kinetic energy, and dipole moment function operators were approximated using third-order $n$-mode expansions. Potential and dipole surfaces were interpolated with cubic splines from CCSD(T)-F12a/cc-pVTZ-F12 single points. The basis functions were chosen as direct products of 1D eigenfunctions (with $OH_f$ eigenfunctions for $OH_b$ due to symmetry), from a symmetry-adapted reference configuration. Low-frequency intermolecular and high-frequency intramolecular vibrations were truncated separately, with an additional energy truncation for all 12 vibrations.[21] The OH-stretching first overtone transitions were estimated to be converged to about 0.5 $cm^{-1}$. Due to the approximations in the 12D model, the water dimer tunneling splittings are not captured well. An 8D (five vibrations, 3 rotations) model was applied to calculate tunneling and $K_a$-rotational structure. Water dimer is an asymmetric rotor with a Ray asymmetry parameter close to the prolate limit and $K_a$ thus serves as a good approximate quantum number. This model, developed within the GENIUSH code, employed the MB-pol potential energy surface and includes derived nuclear spin statistical weights. We applied a rigid-rotor ($J$;$K_a$)-rotational profile computed with PGOPHER to each of the $K_a \rightarrow K_a'$ transitions.[38] We assume that the rotational constants of the ground and vibrationally excited states are identical. In short, the simulated vibrational bands consist of vibrational transitions from the 12D vibrational model, composed with tunneling and $K_a$-structure from the 8D ro-vibrational model, and further composed with rigid-rotor ($J$;$K_a$)-rotational profiles.[21,23] For $\Delta K_a = 0$ transitions, the rigid rotor profile (PGOPHER) is independent of $K_a$.

## RESULTS AND DISCUSSION

In Figure 2, we present the first jet expansion measurement of the $OH_b$-stretching overtone region of the water dimer. The spectrum was recorded with cavity ring-down spectroscopy (CRDS) under jet expansion conditions similar to that used previously to record the other OH-stretching overtone regions.[30]

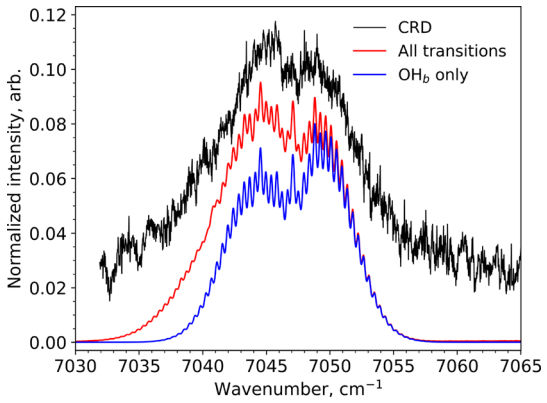


**Figure 2.** Observed and calculated spectrum of the first $OH_b$-stretching overtone band of the water dimer. The blue trace includes only the transition assigned to the $OH_b$-stretching overtone and the red trace also includes contribution from the 4 other vibrational transitions in the regions with oscillator strength higher than $10^{-9}$. Each rotational transition in the simulated spectra has a Lorentzian FWHM of 0.4 $cm^{-1}$ and a temperature of 20 K is used. The computed wavenumbers of the vibrational bands were shifted by +2.9 $cm^{-1}$, to visually match the experimental spectrum.

The band appears like a simple transition with a rotational broadened structure. No individual rotational lines can be observed. The $H_2O$ monomer lines are removed in the spectrum showed in Figure 2. The dip in the center of the band is consistent between different scans (Figure S2) and the peak within the dip is consistently observed. The intensity of the lower energy side is slightly more intense that the higher energy side. In Figure 2, we also show simulated spectra, based on the results tabulated in the Supporting Information of ref


https://doi.org/10.1021/acs.jpca.5c07868
J. Phys. Chem. A XXXX, XXX, XXX−XXX

21, adjusted to $T$ = 20 K. In the vibrational calculations, five vibrational transitions (Table S3) with substantial intensity (oscillator strength larger than $10^{-9}$) are present in the vicinity of the experimentally observed band. The most intense transition is an almost exclusively *a*-type transition assigned to the $OH_b$-stretching overtone. The calculated vibrational band origin is 7045.9 $cm^{-1}$ with an oscillator strength of 5.5 × $10^{-8}$. The *a*-type nature of the transition is to be expected, as the $OH_b$ bond is nearly parallel with the *a*-rotational axis (Table S3), although the direction of the transition dipole moment can change with vibrational excitation.[39] The simulation that includes only this vibrational transition (blue trace in Figure 2) clearly lacks intensity on the low energy side. The simulated band has a maximum on the higher energy side, but the experimental spectrum has a maximum on the lower energy side. However, when the computed 5 vibrational transitions in the region, with an oscillator strength larger than $10^{-9}$, are included (red trace in Figure 2), the intensity to the low energy side of the band increases and the agreement with the experiment improves.

In Figure 3, we illustrate the energy level diagram of the rotation-tunneling states for the dominant transition in the $OH_b$-stretching overtone region. The parallel transitions are shown with arrows with transition wavenumbers indicated.

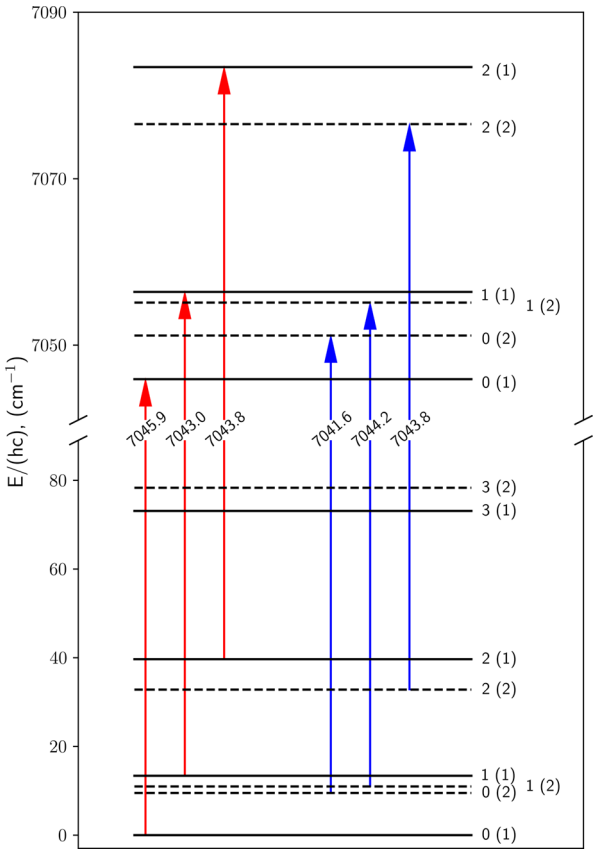


**Figure 3.** Energy level diagram of the rotation-tunneling states associated with $2\nu_{OH_b}$. The parity with respect to the acceptor tunneling splitting is indicated with solid horizontal lines for the (1) components and dashed lines for the (2) component. The parallel VRT transitions included in the simulations are shown with arrows, with red for (1) → (1) transitions and blue for (2) → (2) transitions. The number given is the $K_a$ value and the smallest $J$ value of that transition and the parity is given in parentheses after this number.[21]

Only the large acceptor tunneling splitting is included in our model.[21] The other tunneling splittings are much smaller and split each transition in Figure 3 into three. The intensity distribution between these three arise from the spin statistical weights and are 1:6:1 for $K_a \rightarrow K_a'$ (1) transition and 9:6:9 for $K_a \rightarrow K_a'$ (2) transitions. The index in parentheses denotes the parity of the initial and final states with respect to the acceptor tunneling component. Transitions between states of opposite parity are not allowed.[21] The rotation-tunneling energy levels are given in Table S4. The relative intensity of the transitions in Figure 3, which depend on the spin statistical and Boltzmann weights, are given in Table S5. These VRT transitions lie at lower energies to that of the $K_a$ transition 0 → 0 (1) and the strongest transition does not correspond to the vibrational band origin. The other four vibrational transitions with appreciable intensity in this region have similar rotational-tunneling states and we approximate them to be identical in our simulation. Each of the allowed transitions are convoluted with a rotational band simulated with PGOPHER.[38] The weaker vibrational transitions all lie at lower energies but within 6 $cm^{-1}$ of the main transition. The combined oscillator strength of these 4 transitions is 2.3 × $10^{-8}$, with most of the intensity in two *a*-type bands calculated to be at 7039.7 $cm^{-1}$ (0.51 × $10^{-8}$) and 7042.2 $cm^{-1}$ (1.5 × $10^{-8}$). These contribute to widening the band to lower energies, and change the relative intensity of the lower and higher energy side of the band - improving the agreement with the experimental spectrum. The weaker transitions gain their intensity from coupling to the dominant $OH_b$-stretching transition. In Figure 2, the computed wavenumbers of all five vibrational bands were shifted by +2.9 $cm^{-1}$, to visually match the experimental spectrum. The shift is similar to the ~2 $cm^{-1}$ discrepancy between the corresponding calculated and observed fundamental transition wavenumber. The discrepancies between calculated and experimental transition wavenumbers arise from use of an imperfect potential energy surface and approximation in our vibrational 12D calculations. For the other vibrational OH-stretching first overtone transitions, the optimal transition wavenumber shift was about +6 $cm^{-1}$.[21]

In Figure 4, we show the $2\nu_{OH_b}$ band simulated at different temperatures, with a narrow rotational width of 0.2 $cm^{-1}$. Limited difference is seen between the 15 and 20 K spectrum, and we used 20 K in all simulations. The fact that this band is

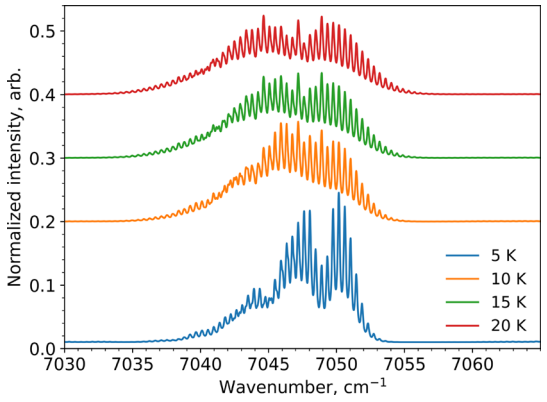


**Figure 4.** Simulation of the first $OH_b$-stretching overtone band in the temperature range from 5 to 20 K. The FWHM of the Lorentzian applied to each transition is 0.2 $cm^{-1}$.


https://doi.org/10.1021/acs.jpca.5c07868
J. Phys. Chem. A XXXX, XXX, XXX−XXX

of *a*-type, is part of the reason why it is difficult to see the underlying structure. The other OH-stretching first overtone transitions are either *b*-type or *a*/*c*-type. Both *b*- and *c*-type bands have transitions spread over $K_a$ sub-bands, which makes it easier to see the VRT structure.[30] The VRT transitions are also split due to the smaller tunneling components, which split each transition into 3 transitions spread by about 1 $cm^{-1}$, based on comparison for the other first OH-stretching overtone bands.[21,30]

In Figure 2, the small peak in the dip can be assigned to the strong Q-branch transition that arise from the $K_a$ transition 1 → 1(2), which we calculated to be at 7044.2 $cm^{-1}$ (Figure 3) and after a shift of +2.9 $cm^{-1}$ is at 7047.1 $cm^{-1}$. The fundamental $K_a$ transition 0 → 0(1), is calculated at 7045.9 $cm^{-1}$ which with the +2.9 $cm^{-1}$ shift moves to 7048.8 $cm^{-1}$ and is the vibrational band origin of the first $OH_b$-stretching transition, $2\nu_{OH_b}$.

We also recorded both the 7030−7065 $cm^{-1}$ region, assigned to the $OH_b$-stretching first overtone, and the region from 7175 to 7240 $cm^{-1}$ under similar experimental conditions (Figure S1). The higher energy region contain previously observed transitions associated with the other three OH-stretching first overtones, the symmetric $2\nu_{OH_+}$ the free $2\nu_{OH_f}$ and the asymmetric, $2\nu_{OH_-}$, with vibrational band origins at 7192.3, 7227 and 7238 $cm^{-1}$, respectively.[21,29,30] These three vibrational bands are of *a*/*c*-type or *b*-type, which give rise to additional sub-bands that are spread over a rather large wavenumber range, in contrast to the concentration of VRT transitions for the almost pure *a*-type of $2\nu_{OH_b}$. We have also simulated spectra in these regions and found good agreement between the relative intensities in the two recorded regions (Figure S2). Based on the calculated oscillator strengths, the intensity in the $2\nu_{OH_b}$ region is about 7% of that for the other 3 OH-stretching transitions.[21]

The intensity of OH-stretching transitions typically fall with an order of magnitude for each subsequent excitation.[40] The cancellation of terms in the dipole moment expansion that is found for the first overtone transition is not expected to the same extend in higher overtones.[26] Thus, the intensity of the second $OH_b$-stretching overtone would be expected to be similar to that of the $2\nu_{OH_b}$ transition. The position of the $3\nu_{OH_b}$ is expected to be around 10344 $cm^{-1}$, based on a simple Birge-Spooner fit of the 2 observed transition and derived Morse energy expression parameters ($\tilde{\omega}$ = 3754 $cm^{-1}$ and $\tilde{\omega}x$ = 76.5 $cm^{-1}$).

In Figure 5, we show simulated spectra of the $2\nu_{OH_b}$ band using different Lorentzian line widths for the individual rotational transition in PGOPHER. The best visual match with the observed spectrum is seen using a full width at half maximum (FWHM) Lorentzian width of about 0.8 $cm^{-1}$. Simulated spectra with significantly lower widths lead to rotational structure that would have been visible in the experimental spectrum. With a larger width, the dip near the center of the band disappears. We therefore estimate that the FWHM line width is about 0.8 $cm^{-1}$, which corresponds to a lifetime of about 7 ps. This estimate does not take into account the additional tunneling splitting not included in the simulations. Therefore, the actual line width could be somewhat smaller, but not too much smaller, otherwise rotational structure in the observed spectra would be visible.

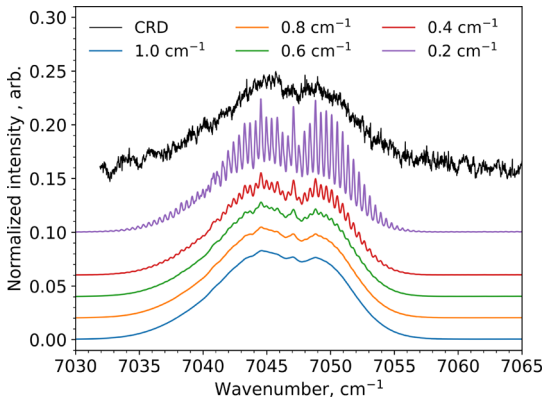


**Figure 5.** Simulation of the first $OH_b$-stretching overtone including all five vibrational transitions from Table S3 and VRT transitions from Table S5. The Lorentzian FWHM of the individual rotational lines is increased from 0.2 to 1.0 $cm^{-1}$. The temperature was fixed at 20 K. The computed wavenumbers of the vibrational bands were shifted by +2.9 $cm^{-1}$, to visually match the experimental spectrum. The experimental CRD spectrum is shown in black.

Halving the line width to 0.4 $cm^{-1}$ corresponds to a lifetime of about 14 ps, and we estimate the lifetime of $2\nu_{OH_b}$ to be about 10 ps. In comparison, the line widths of the other three OH-stretching overtones have been estimated to be in the range 0.05 to 0.25 $cm^{-1}$, which corresponds to somewhat longer lifetimes of 20−100 ps.[30] It is not surprising that exciting the $OH_b$-stretching transition would lead to a relatively shorter lifetime, due to the expected stronger coupling with other excited and dissociative states. In comparison for weaker bound complexes, where the vibrational coupling is likely much less, the lifetime can be on the order of ns for excitation in the same spectral region, as has been determined for $H_2O$−Ar and $H_2O$−Kr.[41]

## CONCLUSIONS

We have recorded the spectrum of water dimer in the 7030−7065 $cm^{-1}$ region using jet expansion cavity ring-down spectroscopy. We detect a characteristic *a*-type band that we assign to the $OH_b$-stretching first overtone. The observed band is simulated well based on a full-dimensional ro-vibrational calculation. The overlap of many closely lying ro-vibrational transitions, even at the cold temperature of the jet (about 20 K), gives rise to a relatively unstructured broad band with no individual rotational lines visible. Based on the comparison with the 12D calculation and the simulated spectrum the experimental $OH_b$-stretching first overtone vibrational band origin is 7049 $cm^{-1}$, and the lifetime is estimated to be about 10 ps. The bound OH-stretching ($OH_b$) vibration is challenging to describe both with regards to the ab initio method used to calculate the potential energy and dipole moment surfaces as well as describing couplings within the vibrational model. The fact that the calculations agree well with both the previously recorded fundamental and the present first $OH_b$-stretching transition validates the robustness of the theoretical description of the water dimer.

## ASSOCIATED CONTENT

### Supporting Information

The Supporting Information is available free of charge at https://pubs.acs.org/doi/10.1021/acs.jpca.5c07868.



https://doi.org/10.1021/acs.jpca.5c07868
J. Phys. Chem. A XXXX, XXX, XXX−XXX

Contains further experimental CRDS spectra and tables with theoretical details (PDF)

## AUTHOR INFORMATION


### Corresponding Authors

**Henrik G. Kjaergaard** − *Department of Chemistry, University of Copenhagen, DK-2100 Copenhagen, Denmark;* orcid.org/0000-0002-7275-8297; Phone: +45-35320334; Email: hgk@chem.ku.dk; Fax: +45-35320322

**Clément Lauzin** − *Institute of Condensed Matter and Nanosciences, Université catholique de Louvain, B-1348 Louvain-la-Neuve, Belgium;* orcid.org/0000-0001-5044-5137; Email: clement.lauzin@uclouvain.be

### Authors

**Emil Vogt** − *Department of Chemistry, University of Copenhagen, DK-2100 Copenhagen, Denmark;* orcid.org/0000-0003-3335-9813

**Alexandr S. Bogomolov** − *Institute of Condensed Matter and Nanosciences, Université catholique de Louvain, B-1348 Louvain-la-Neuve, Belgium;* orcid.org/0000-0002-6675-0969

Complete contact information is available at: https://pubs.acs.org/10.1021/acs.jpca.5c07868


### Notes

The authors declare no competing financial interest.

## ACKNOWLEDGMENTS

We thank the "Fonds de la Recherche Scientifique"(FNRS, F.4038.24), the Novo Nordisk Foundation (NNF22OC0080193), and the Carlsberg Foundation (CF24-1034) for funding this research. We also thank the High Performance Computing Center at the University of Copenhagen for providing computational resources. CL acknowledges the SQUARES research unit of Université Libre de Bruxelles for loan of the FANTASIO setup. ASB is funded by the European Union. Views and opinions expressed are however those of the authors only and do not necessarily reflect those of the European Union or the European Research Executive Agency (REA). Neither the European Union nor the granting authority can be held responsible for them.

## REFERENCES


(1) Vaida, V.; Daniel, J. S.; Kjaergaard, H. G.; Goss, L. M.; Tuck, A. F. Atmospheric absorption of near infrared and visible solar radiation by the hydrogen bonded water dimer. *Q. J. R. Meteorol. Soc.* **2001**, *127*, 1627−1643.

(2) Simonova, A. A.; Ptashnik, I. V.; Shine, K. P. Semi-empirical water dimer model of the water vapour self-continuum within the IR absorption bands. *J. Quant. Spectrosc. Radiat. Transfer* **2024**, *329*, 109198.

(3) Vogt, E.; Kjaergaard, H. G. Vibrational Spectroscopy of the Water Dimer at Jet-Cooled and Atmospheric Temperatures. *Annu. Rev. Phys. Chem.* **2022**, *73*, 209−231.

(4) Van Thiel, M.; Becker, E. D.; Pimentel, G. C. Infrared studies of hydrogen bonding of water by the matrix isolation technique. *J. Chem. Phys.* **1957**, *27*, 486−490.

(5) Buckingham, A.; Del Bene, J.; McDowell, S. The hydrogen bond. *Chem. Phys. Lett.* **2008**, *463*, 1−10.

(6) Arunan, E.; Desiraju, G. R.; Klein, R. A.; Sadlej, J.; Scheiner, S.; Alkorta, I.; Clary, D. C.; Crabtree, R. H.; Dannenberg, J. J.; Hobza, P.; Kjaergaard, H. G.; Legon, A. C.; Mennucci, B.; Nesbitt, D. J. Defining the hydrogen bond: An account (IUPAC Technical Report). *Pure Appl. Chem.* **2011**, *83*, 1619−1636.

(7) Arunan, E.; Desiraju, G. R.; Klein, R. A.; Sadlej, J.; Scheiner, S.; Alkorta, I.; Clary, D. C.; Crabtree, R. H.; Dannenberg, J. J.; Hobza, P.; Kjaergaard, H. G.; Legon, A. C.; Mennucci, B.; Nesbitt, D. J. Definition of the hydrogen bond (IUPAC Recommendations 2011). *Pure Appl. Chem.* **2011**, *83*, 1637−1641.

(8) Huisken, F.; Kaloudis, M.; Kulcke, A. Infrared spectroscopy of small size-selected water clusters. *J. Chem. Phys.* **1996**, *104*, 17−25.

(9) Buck, U.; Huisken, F. Infrared spectroscopy of size-selected water and methanol clusters. *Chem. Rev.* **2000**, *100*, 3863−3890.

(10) Paul, J. B.; Collier, C. P.; Saykally, R. J.; Scherer, J. J.; O'Keefe, A. Direct Measurement of Water Cluster Concentrations by Infrared Cavity Ringdown Laser Absorption Spectroscopy. *J. Phys. Chem. A* **1997**, *101*, 5211−5214.

(11) Bouteiller, Y.; Perchard, J. The vibrational spectrum of $(H_2O)_2$: Comparison between anharmonic ab initio calculations and neon matrix infrared data between 9000 and 90 $cm^{-1}$. *Chem. Phys.* **2004**, *305*, 1−12.

(12) Nelander, B. The intramolecular fundamentals of the water dimer. *J. Chem. Phys.* **1988**, *88*, 5254−5256.

(13) León, I.; Montero, R.; Castaño, F.; Longarte, A.; Fernández, J. A. Mass-resolved infrared spectroscopy of complexes without chromophore by nonresonant femtosecond ionization detection. *J. Phys. Chem. A* **2012**, *116*, 6798−6803.

(14) León, I.; Montero, R.; Longarte, A.; Fernández, J. A. Revisiting the spectroscopy of water dimer in jets. *J. Phys. Chem. Lett.* **2021**, *12*, 1316−1320.

(15) Kjaergaard, H. G.; Garden, A. L.; Chaban, G. M.; Gerber, R. B.; Matthews, D. A.; Stanton, J. F. Calculation of vibrational transition frequencies and intensities in water dimer: Comparison of different vibrational approaches. *J. Phys. Chem. A* **2008**, *112*, 4324−4335.

(16) Low, G. R.; Kjaergaard, H. G. Calculation of OH-stretching band intensities of the water dimer and trimer. *J. Chem. Phys.* **1999**, *110*, 9104−9115.

(17) Schofield, D. P.; Kjaergaard, H. G. Calculated OH-stretching and HOH-bending vibrational transitions in the water dimer. *Phys. Chem. Chem. Phys.* **2003**, *5*, 3100−3105.

(18) Leforestier, C.; Gatti, F.; Fellers, R. S.; Saykally, R. J. Determination of a flexible (12D) water dimer potential via direct inversion of spectroscopic data. *J. Chem. Phys.* **2002**, *117*, 8710−8722.

(19) Leforestier, C.; Szalewicz, K.; van der Avoird, A. Spectra of water dimer from a new *ab initio* potential with flexible monomers. *J. Chem. Phys.* **2012**, *137*, 014305.

(20) Wang, X. G.; Carrington, T. Computing excited OH stretch states of water dimer in 12D using contracted intermolecular and intramolecular basis functions. *J. Chem. Phys.* **2023**, *158*, 084107.

(21) Vogt, E.; Simkó, I.; Császár, A. G.; Kjaergaard, H. G. Quantum Chemical Investigation of the Cold Water Dimer Spectrum in the First OH-Stretching Overtone Region Provides a New Interpretation. *J. Phys. Chem. A* **2023**, *127*, 9409−9418.

(22) Jing, A.; Wang, X.-G.; Carrington, T. J.; Szalewicz, K. Breaking the 1 $cm^{-1}$ Discrepancy with Experiment Limit in First-Principles Calculations of Water Dimer Vibration−Rotation−Tunneling Spectra. *J. Phys. Chem. Lett.* **2025**, *16*, 10923−10931.

(23) Vogt, E.; Simkó, I.; Császár, A. G.; Kjaergaard, H. G. Reduced-dimensional vibrational models of the water dimer. *J. Chem. Phys.* **2022**, *156*, 164304.

(24) Perchard, J. P. Anharmonicity and hydrogen bonding. II. A near infrared study of the water trapped in nitrogen matrix. *Chem. Phys.* **2001**, *266*, 109−124.

(25) Perchard, J. P. Anharmonicity and hydrogen bonding. III. Analysis of the near infrared spectrum of water trapped in argon matrix. *Chem. Phys.* **2001**, *273*, 217−233.

(26) Kjaergaard, H. G.; Low, G. R.; Robinson, T. W.; Howard, D. L. Calculated OH-Stretching Vibrational Transitions in the Water-Nitrogen and Water-Oxygen Complexes. *J. Phys. Chem. A* **2002**, *106*, 8955−8962.

(27) Mackeprang, K.; Kjaergaard, H. G.; Salmi, T.; Hänninen, V.; Halonen, L. The effect of large amplitude motions on the transition frequency redshift in hydrogen bonded complexes: A physical picture. *J. Chem. Phys.* **2014**, *140*, 184309.
(28) Mackeprang, K.; Hänninen, V.; Halonen, L.; Kjaergaard, H. G. The effect of large amplitude motions on the vibrational intensities in hydrogen bonded complexes. *J. Chem. Phys.* **2015**, *142*, 094304.
(29) Nizkorodov, S. A.; Ziemkiewicz, M.; Nesbitt, D. J.; Knight, A. E. W. Overtone spectroscopy of $H_2O$ clusters in the $\nu_{OH}$=2 manifold: Infrared-ultraviolet vibrationally mediated dissociation studies. *J. Chem. Phys.* **2005**, *122*, 194316.
(30) Suas-David, N.; Vanfleteren, T.; Földes, T.; Kassi, S.; Georges, R.; Herman, M. The water dimer investigated in the 2OH spectral range using cavity ring-down spectroscopy. *J. Phys. Chem. A* **2015**, *119*, 10022−10034.
(31) Hippler, M.; Oeltjen, L.; Quack, M. High-Resolution Continuous-Wave-Diode Laser Cavity Ring-Down Spectroscopy of the Hydrogen Fluoride Dimer in a Pulsed Slit Jet Expansion: Two Components of the N = 2 Triad near 1.3 $\mu$m. *J. Phys. Chem. A* **2007**, *111*, 12659−12668.
(32) Kollipost, F.; Papendorf, K.; Lee, Y.-F.; Lee, Y.-P.; Suhm, M. A. Alcohol dimers − how much diagonal OH anharmonicity? *Phys. Chem. Chem. Phys.* **2014**, *16*, 15948−15956.
(33) Herman, M.; Didriche, K.; Hurtmans, D.; Kizil, B.; Macko, P.; Rizopoulos, A.; Poucke, P. V. FANTASIO: a versatile experimental set-up to investigate jet-cooled molecules. *Mol. Phys.* **2007**, *105*, 815−823.
(34) Didriche, K.; Lauzin, C.; Földes, T.; de Ghellinck D'Elseghem Vaernewijck, X.; Herman, M. The FANTASIO+ set-up to investigate jet-cooled molecules: focus on overtone bands of the acetylene dimer. *Mol. Phys.* **2010**, *108*, 2155−2163.
(35) Bogomolov, A. S.; Glorieux, R.; Herman, M.; Corbo, T.; Collignon, S.; Hays, B. M.; Lederer, D.; Moazzen-Ahmadi, N.; Libert, A.; Tomasetti, B.; Fréreux, J.; Lauzin, C. Improvements on the FANTASIO set-up and new spectroscopic results concerning the Ar-H2O van der Waals complex in the 2OH overtone region. *Mol. Phys.* **2025**, *123*, e2413417.
(36) Bogomolov, A.; Roucou, A.; Bejjani, R.; Herman, M.; Moazzen-Ahmadi, N.; Lauzin, C. The rotationally resolved symmetric 2OH excitation in $H_2O$-$CO_2$ observed using pulsed supersonic expansion and CW-CRDS. *Chem. Phys. Lett.* **2021**, *774*, 138606.
(37) Gordon, I. E.; Rothman, L. S.; Hargreaves, R. J.; Hashemi, R.; Karlovets, E. V.; Skinner, F. M.; Conway, E. K.; Hill, C.; Kochanov, R. V.; Tan, Y.; Wcisło, P.; Finenko, A. A.; Nelson, K.; Bernath, P. F.; Birk, M.; Boudon, V.; Campargue, A.; Chance, K. V.; Coustenis, A.; Drouin, B. J.; Flaud, J.-M.; Gamache, R. R.; Hodges, J. T.; Jacquemart, D.; Mlawer, E. J.; Nikitin, A. V.; Perevalov, V. I.; Rotger, M.; Tennyson, J.; Toon, G. C.; Tran, H.; Tyuterev, V. G.; Adkins, E. M.; Baker, A.; Barbe, A.; Canè, E.; Császár, A. G.; Dudaryonok, A.; Egorov, O.; Fleisher, A. J.; Fleurbaey, H.; Foltynowicz, A.; Furtenbacher, T.; Harrison, J. J.; Hartmann, J.-M.; Horneman, V. -M.; Huang, X.; Karman, T.; Karns, J.; Kassi, S.; Kleiner, I.; Kofman, V.; Kwabia−Tchana, F.; Lavrentieva, N. N.; Lee, T. J.; Long, D. A.; Lukashevskaya, A. A.; Lyulin, O. M.; Makhnev, V. Y.; Matt, W.; Massie, S. T.; Melosso, M.; Mikhailenko, S. N.; Mondelain, D.; Müller, H. S. P.; Naumenko, O. V.; Perrin, A.; Polyansky, O. L.; Raddaoui, E.; Raston, P. L.; Reed, Z. D.; Rey, M.; Richard, C.; Tóbiás, R.; Sadiek, I.; Schwenke, D. W.; Starikova, E.; Sung, K.; Tamassia, F.; Tashkun, S. A.; Vander Auwera, J.; Vasilenko, I. A.; Vigasin, A. A.; Villanueva, G. L.; Vispoel, B.; Wagner, G.; Yachmenev, A.; Yurchenko, S. N. The HITRAN2020 molecular spectroscopic database. *J. Quant. Spectrosc. Radiat. Transfer* **2022**, *277*, 107949.
(38) Western, C. M. PGOPHER: A program for simulating rotational, vibrational and electronic spectra. *Journal of Quantitative Spectroscopy and Radiative Transfer* **2017**, *186*, 221−242.
(39) Ishiuchi, S.-i.; Fujii, M.; Robinson, T. W.; Miller, B. J.; Kjaergaard, H. G. Vibrational Overtone Spectroscopy of Phenol and Its Deuterated Isotopomers. *J. Phys. Chem. A* **2006**, *110*, 7345−7354.
(40) Miller, B. J.; Du, L.; Steel, T. J.; Paul, A. J.; Södergren, A. H.; Lane, J. R.; Henry, B. R.; Kjaergaard, H. G. Absolute Intensities of NH-Stretching Transitions in Dimethylamine and Pyrrole. *J. Phys. Chem. A* **2012**, *116*, 290−296.
(41) Herman, M.; Földes, T.; Didriche, K.; Lauzin, C.; Vanfleteren, T. Overtone spectroscopy of molecular complexes containing small polyatomic molecules. *Int. Rev. Phys. Chem.* **2016**, *35*, 243−295.




https://doi.org/10.1021/acs.jpca.5c07868
J. Phys. Chem. A XXXX, XXX, XXX−XXX